Benefits of cascaded nonlinear dynamics in hybrid fibers for low-noise supercontinuum generation

Pascal Hänzi,[1,*] Benoît Sierro,[1] Zhixin Liu,[2]
Valerio Romano,[1,3] Anupamaa Rampur,[1]
and Alexander M. Heidt[1]

[1]*Institute of Applied Physics, University of Bern, Sidlerstrasse 5, 3012 Bern, Switzerland*
[2]*Department of Electronic and Electrical Engineering, University College London, UK*
[3]*Bern University of Applied Sciences BUAS, Applied Laser-, Photonics- and Surface Technologies ALPS, Pestalozzistrasse 20, 3400 Burgdorf, Switzerland*
*pascal.haenzi@unibe.ch

Abstract: The recent development of fiber supercontinuum (SC) sources with ultra-low noise levels has been instrumental in advancing the state-of-the-art in a wide range of research topics. However, simultaneously satisfying the application demands of maximizing spectral bandwidth and minimizing noise is a major challenge that so far has been addressed with compromise, found by fine-tuning the characteristics of a single nonlinear fiber transforming the injected laser pulses into a broadband SC. In this work, we investigate a hybrid approach that splits the nonlinear dynamics into two discrete fibers optimized for nonlinear temporal compression and spectral broadening, respectively. This introduces new design degrees of freedom, making it possible to select the best fiber for each stage of the SC generation process. With experiments and simulations we study the benefits of this hybrid approach for three common and commercially available highly nonlinear fiber (HNLF) designs, focusing on flatness, bandwidth and relative intensity noise of the generated SC. In our results, hybrid all-normal dispersion (ANDi) HNLF stand out as they combine the broad spectral bandwidths associated with soliton dynamics with extremely low noise and smooth spectra known from normal dispersion nonlinearities. Hybrid ANDi HNLF are a simple and low-cost route for implementing ultra-low noise SC sources and scaling their repetition rate for various applications such as biophotonic imaging, coherent optical communications, or ultrafast photonics.

1. Introduction

Low-noise fiber supercontinuum (SC) sources, providing broad spectral bandwidths and high brightness combined with excellent stability and coherence, have been the key-enabling technology for recent advancements of the state-of-the-art in several applications such as hyperspectral and multimodal nonlinear imaging, near-field optical microscopy, optical coherence tomography at the shot-noise limit, and ultrafast photonics [1–8]. Ultra-low amplitude- and phase-noise performance is also an essential requirement for applications in coherent optical communications and photonic signal processing based on nonlinear spectral broadening of frequency combs with gigahertz-range repetition rates [9,10]. As the noise properties of the generated SC light depend critically on the dispersion and birefringence engineering of the employed nonlinear fiber, various designs for low-noise SC generation have been proposed and implemented [11–15].

The nonlinear transformation of a narrowband ultrafast laser into a broadband SC in a highly nonlinear fiber (HNLF) is often a two-stage process: higher-order soliton compression is followed

by additional nonlinear broadening dynamics, whose details depend on the dispersion design of the particular HNLF in use [16]. Typically, a single HNLF is used for SC generation, such that simultaneously satisfying the application demands of maximizing spectral bandwidth and minimizing noise has remained a major challenge, as they often place diametrically opposing constraints on the nonlinear fiber design [1].

In this work, we investigate the benefits of an hybrid fiber approach for ultra-low noise SC generation, which splits the nonlinear dynamics into two discrete fibers, both individually optimized for each stage. Inspired by early works with dispersion flattened and dispersion decreasing fibers [17–19], hybrid fibers consist of a short piece of anomalous dispersion single-mode fiber (SMF) fusion spliced to the input side of a highly nonlinear fiber (Fig. 1). When a femtosecond pulse is injected, it experiences cascaded nonlinear dynamics, where in the SMF section nonlinear soliton compression shortens the pulse duration to the few-cycle regime and substantially increases the peak power, while in the subsequent HNLF section a broadband SC spectrum is generated. Hybrid fibers give rise to a range of new possibilities in nonlinear fiber optics as they allow a free choice of a HNLF design that ideally supports the desired low-noise nonlinear conversion processes while simultaneously harnessing the benefits offered by an optimized soliton compression process, which maximizes the generated SC bandwidth.
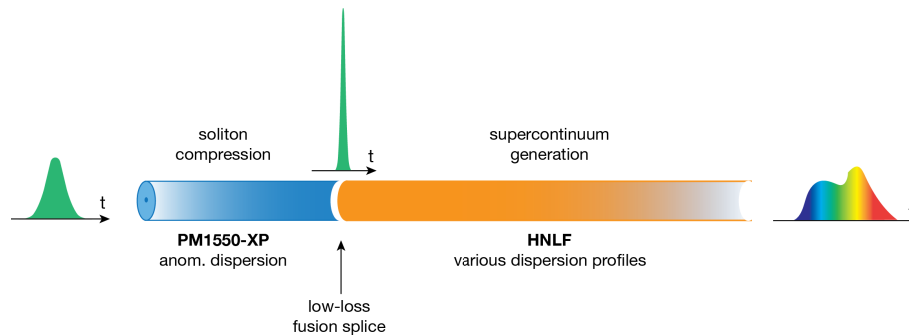

Fig. 1. Hybrid fiber concept. The hybrid version of a particular highly nonlinear fiber (HNLF) consists of a short piece of single mode fiber (here: PM1550-XP), exhibiting anomalous dispersion at the pump wavelength, fusion spliced to the input side of the HNLF. This induces cascaded nonlinear dynamics, where in the first section nonlinear soliton compression shortens the duration and increases the peak power of the input pulse, while in the subsequent HNLF section a broadband SC spectrum is generated by nonlinear dynamics that depend on the dispersion profile of the particular HNLF.

One of those possibilities we pursued in our previous work, where we applied the hybrid fiber concept to an all-normal dispersion (ANDi) HNLF [20]. By cascading soliton compression and optical wave breaking, the hybrid ANDi HNLF combines the most beneficial aspects of nonlinear dynamics in both anomalous and normal dispersion regimes, resulting in an ultra-low noise, octave-spanning fiber SC source with near-perfect phase coherence and spectrally resolved relative intensity noise (RIN) as low as 0.05%. This is an order of magnitude lower than prior art and approaching the theoretical limits close to the pump laser noise.

Here we extend this hybrid fiber concept to other common and commercially available HNLF and compare their performance under identical pumping conditions using a standard commercial Erbium(Er):fiber laser emitting 100 fs pulses at 1550 nm. The HNLF are chosen such that they form a representative set of the most common types of dispersion designs used for SC generation and, therefore, are ideally suited to experimentally study the influence of the fiber dispersion design on spectral bandwidth, flatness, and noise characteristics of the resulting SC. For this purpose, we present a detailed comparison of spectrally resolved RIN of the SC light generated

in these different HNLF designs, both for directly pumped and hybrid fiber versions. Only polarization-maintaining fibers are considered, as high birefringence suppresses noise arising from the nonlinear coherent coupling of the two orthogonal eigenmodes [1,21].

Our results demonstrate that the hybrid approach leads to (i) broader and (ii) flatter SC spectra with reduced fine-structure for all tested HNLF designs in comparison to the respective directly pumped HNLF. We link these benefits to the optimized nonlinear dynamics in the hybrid fiber maintaining a cleaner temporal pulse shape during the nonlinear transformation. In contrast, we show that the ultra-low noise performance of the hybrid ANDi fiber SC source cannot be reproduced with conventional HNLF designs pumped near their zero dispersion wavelengths, which exhibit on average about an order-of-magnitude higher spectrally resolved RIN. These results highlight the decisive role of the HNLF dispersion engineering for ultra-low noise, high-quality SC generation, even when few-cycle pump pulses are employed. Owing to its simplicity and its scalability to high repetition rates, the hybrid fiber approach is readily transferable to various laser platforms and could enhance the performance of high performance laser applications where low intensity and phase noise critically matter.

2. Methods and materials

2.1. Experimental setup and RIN measurement

The experimental setup used to generate and analyze the SC is shown in Fig. 2. An ultrafast Er:fiber laser (Toptica FemtoFiber pro) with a spectrum centered at 1560 nm delivers a 110 fs pump pulse train with f_{rep} = 40 MHz repetition rate and polarization extinction ratio (PER) of 30 dB. A half-wave plate is used to align the polarization state of the input pulses to the fiber's principal birefringence axes. The pump pulses are coupled into the fiber under test (FUT) by an aspheric lens with focal length chosen to match the mode field diameter of the fiber, resulting in a maximum coupled average power of 210 mW. This corresponds to a peak power of 33 kW, calculated using the real pulse shape emitted by the laser measured by time-domain ptychography. The generated SC spectra are recorded using two optical spectrum analyzer (OSA) (Yokogawa AQ6370 for λ<1700 nm and AQ6375 for λ>1700 nm). A polarizer is inserted in the beam path in order to analyze the polarization extinction ratio (PER) of the SC, and also serves for converting possible polarization state fluctuations into amplitude noise that can be detected using the subsequent relative intensity noise (RIN) measurement system.
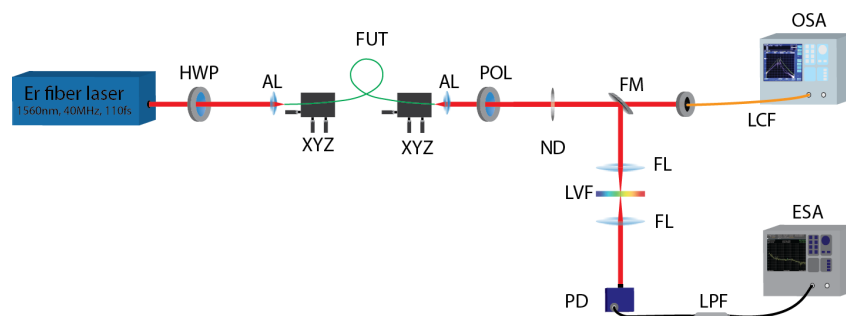

Fig. 2. Schematic setup for supercontinuum generation and RIN measurement. HWP: half wave plate; AL: aspheric lens; XYZ: three axis translation stage; FUT: fiber under test; POL: polarizer; ND: neutral density filter; FM: flip mirror; LCF: large core fiber patch cord; OSA: optical spectrum analyzer; FL: focusing lens; LVF: linear variable filter 1.3 μm - 2.6 μm; PD: photo diode; LPF: low pass filter (< 21 MHz); ESA: electronic spectrum analyzer.

We measure relative intensity noise (RIN) in the frequency domain as this is the standard method most frequently used in the noise characterization of optical frequency combs and

ultrafast lasers [22,23]. The pulse train is detected by a slow amplified photodiode (Thorlabs PDA10D2, bandwidth DC - 25 MHz, 900 - 2600 nm spectral range, 5 kV/A transimpedence gain) and analyzed using an electronic spectrum analyzer (ESA) (Keysight E5052B and Signal Hound USB-SA44B) in the baseband from 10 Hz up to the Nyquist frequency of $f_{rep}/2 = 20$ MHz. The photodiode signal is filtered by an electrical 21 MHz low-pass filter to avoid saturation of the electronic spectrum analyzer (ESA) at the pulse repetition rate as well as a DC block capacitor with cut-off frequency <3 Hz. This procedure gives access to the pure amplitude noise power spectral density (PSD) without any phase noise contributions. Integration of the square root of the measured PSD over the baseband then yields the total relative intensity noise (RIN) of the pulse train, i.e. all quoted RIN values in this paper refer to a 10 Hz - 20 MHz integration range.

The spectrally resolved relative intensity noise (RIN) is measured in the same way, but the SC is first passed through a linear variable bandpass filter with 20 nm bandwidth covering the range 1300 - 2600 nm (Vortex Optical Coatings, UK) before the photodiode detection. Additional discrete bandpass filters with similar bandwidths cover the shorter wavelengths below 1300 nm.

For each measured relative intensity noise (RIN) value we also determine the electronic noise floor of the detection system so that it can be easily determined whether the detected fluctuations truly stem from the SC pulse train or are limited by the noise of the measurement apparatus. We obtain a typical electronic noise floor of 0.03 % RIN (or -140 dBc/Hz at high Fourier frequencies). This is higher than typically used for ultrafast laser characterization, because we tuned the system not for high sensitivity at the peak wavelength, but for providing a similar noise floor over as much spectral bandwidth and signal levels as possible.

We note that both spectral bandpass and polarization filters are important to fully characterize the SC stability. As the intensity noise of SC sources is typically anti-correlated across the spectrum, omitting these filters conceals noise features by averaging fluctuations of anti-correlated portions of the spectrum leading to lower apparent RIN values. For this reason, our measurements are not directly comparable to studies that did not implement this spectral and polarization selectivity.

2.2. Fibers

The fibers used in this work are all commercial polarization-maintaining step-index fibers. PM1550-XP fiber (Coherent-Nufern) is used to study the hybrid fiber approach exploiting initial pulse shortening via nonlinear soliton pre-compression, while broadband SC spectra are generated in three different germanium-doped HNLF obtained from different manufacturers. Figure 3 shows the pump source spectrum in relation to the measured group velocity dispersion profiles of the fibers.

The HNLF are chosen such that they form a representative set of the most common types of fibers used for SC generation. While HNLF-AD and HNLF-ND exhibit a single zero-dispersion wavelength (ZDW) and provide low anomalous and normal dispersion at the pump wavelength, respectively, HNLF-ANDi has an all-normal dispersion profile. Therefore, the fibers are ideally suited to experimentally clarify the influence of the fiber dispersion profile on the noise characteristics of the resulting SC under identical pumping conditions.

A summary of geometric, linear and nonlinear optical parameters of the fibers used in this work is given in Table 1. HNLF-AD (sold by FORC-Photonics as HNLF DS) exhibits anomalous dispersion at the pump wavelength, with a ZDW of 1.47 μm and $D = 3.3$ ps/(nm km) at 1550 nm. Its MFD is given as 4.2 μm by the manufacturer and we estimate its nonlinear coefficient to $\gamma = 10.3$ (Wm)$^{-1}$. Due to a slightly elliptic core the fiber has a group birefringence of 0.9×10^{-4} relative index units (RIU). On the other hand, HNLF-ND (marketed by OFS as HNLF-PM-M2) provides normal dispersion over the pump spectrum, with a ZDW of 1.62 μm and $D = -1.07$ ps/(nm km) at 1550 nm. Birefringence of 2.8×10^{-4} RIU is introduced by an
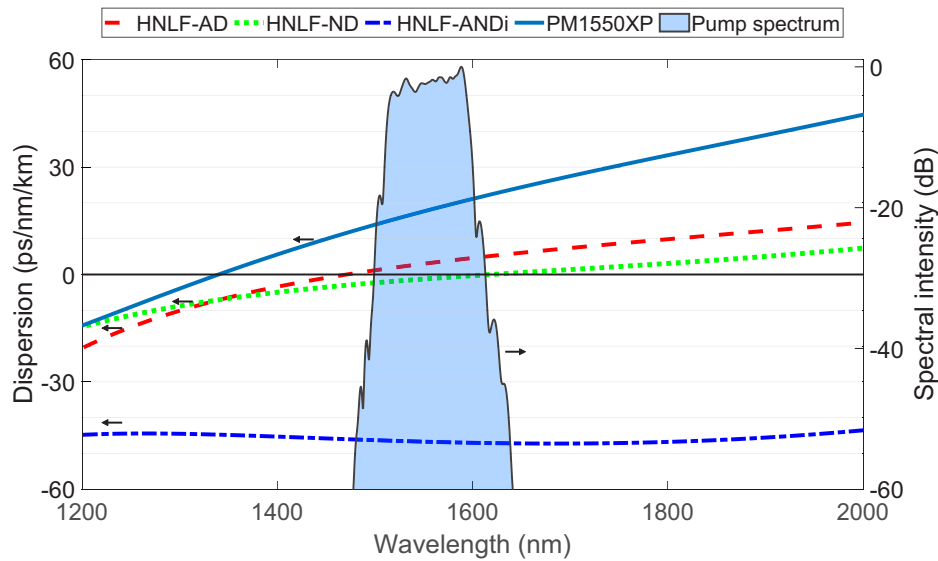
Fig. 3. Measured dispersion curves of HNLF-AD, HNLF-ND, HNLF-ANDi, and PM1550-XP in relation to the measured spectrum of the Er:fiber femtosecond laser.

elliptic core, and MFD as well as nonlinear coefficient are similar to HNLF-AD. Finally, HNLF-ANDi (Coherent-Nufern PM2000D) exhibits relatively strong and flat all-normal dispersion over the entire wavelength region of interest with $D = -46.7\,\text{ps/(nm\,km)}$ at 1550 nm [24]. Its birefringence of 0.2×10^{-4} RIU is introduced by a panda structure, and it provides about 30% higher nonlinearity compared to the other HNLFs used in this study.

Table 1. Geometric, linear, and nonlinear properties of the fibers used in this work. All values except ZDW are given for a wavelength of 1550 nm.

Fiber	MFD [µm]	ZDW [nm]	Dispersion [ps/nm/km]	Group birefringence	Nonlinearity [W^{-1} km^{-1}]
PM1550-XP	10.1	1340	18	4.6×10^{-4}	1.4
HNLF-AD	4.2	1469	3.3	0.9×10^{-4}	10.3
HNLF-ND	4	1620	-1.07	2.8×10^{-4}	10.5
HNLF-ANDi	3.5	All normal	-46.7	0.2×10^{-4}	13.3

2.3. Soliton pre-compression in hybrid fibers

It is well known that shorter input pulses reduce SC noise and improve coherence in any fiber design [16,25]. A convenient and compact way to shorten the input pulse before it enters the HNLF is the fabrication of a hybrid fiber, which exploits nonlinear soliton compression in a short piece of SMF fusion spliced to the input side of the HNLF (Fig. 1). We select PM-1550XP for the pre-compression stage, because in this fiber the input pulses delivered by the Er:fiber laser form a soliton of order $N \simeq 4$, which yields a good compromise between compression factor and compressed pulse quality [26].

The length of PM1550-XP fiber required to reach the minimum compressed pulse duration is determined via a cut-back measurement, and a length of 5.7 cm is chosen for the fabrication of all hybrid fibers used in this work. Figure 4(c) illustrates the effect of the soliton compression by comparing the original 109.3 fs Er:fiber laser pulse with the compressed soliton of 22.9 fs duration

obtained at the output of the 5.7 cm long piece of PM1550-XP. Both pulses are retrieved from a full spectro-temporal measurement by time-domain ptychography [27]. Due to the temporal compression the peak power increases to 150 kW. Taking the splice loss of ∼ 1 dB into account (discussed below), we estimate the pulses to enter the HNLF section with a peak power of about 120 kW.
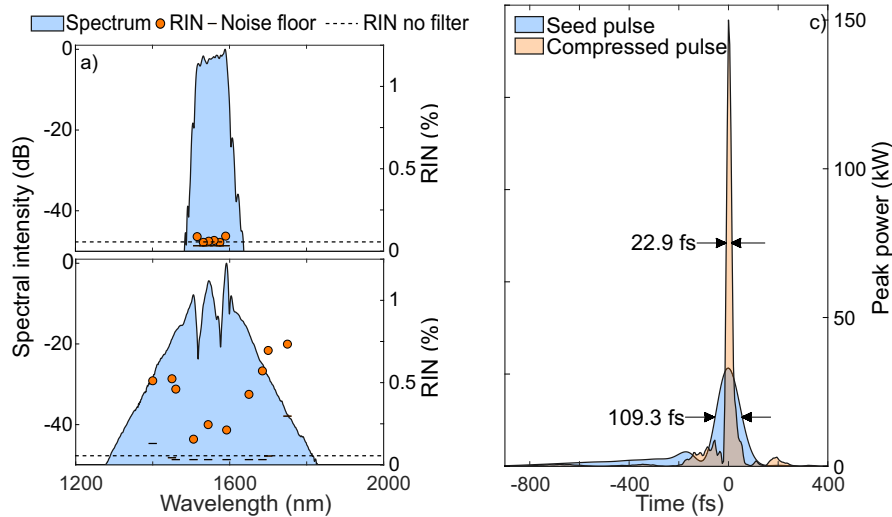

Fig. 4. Spectrum and spectrally resolved RIN of the a) uncompressed Er:fiber femtosecond laser, and b) the compressed soliton after propagation through 5.7 cm of PM1550-XP. Left scale: measured (solid blue) spectrum; right scale: measured spectrally resolved RIN (circles) with corresponding noise floor (-). The dashed line indicates the overall RIN without any spectral filtering applied. (b) Pulse shape of the Er: fiber femtosecond laser and the compressed soliton, measured using time-domain ptychography.

The stability of both pump laser and compressed soliton pulse train is evaluated by performing RIN measurements. For the Er:fiber laser a total RIN of 0.05% (10 Hz - 20 MHz) is obtained, and spectrally resolved measurements provide similar values over the entire bandwidth of the laser (Fig. 4(a)). For the compressed 23 fs soliton pulse train, the spectrally resolved measurements reveal an increased RIN of about 0.2% in the center and exceeding 0.6% at the edges of the nonlinearly broadened spectrum (Fig. 4(b)). However, when the spectral filter is removed, the RIN drops to a value 0.05%, i.e. equal to the pump laser. This behaviour is the result of nonlinear spectral broadening by self-phase modulation (SPM), which converts fluctuations of the input pulse peak power to spectral "breathing" with zones of anti-correlated spectral intensity noise [28]. As shown by a recent numerical study, these SPM-induced local spectral fluctuations do not have any significant impact on the stability or quality of the unfiltered compressed pulses in the time domain, such that they maintain the same RIN as the pump laser [29]. Hence, in the hybrid approach the temporal compression and peak power enhancement of the input pulse is obtained without incurring a significant noise penalty.

We fabricate hybrid versions for each of the three HNLF detailed in Section 2.2. The PM1550-XP fiber is cleaved to a length of 5.7 ± 0.2 cm and directly fusion spliced to the respective HNLF. Despite the large MFD mismatch between PM1550-XP and the HNLFs we routinely achieve ≤ 1 dB splice loss using the thermally expanding core technique. By increasing the arc duration of our fusion splicer, thermal diffusion of germanium ions from the core into the cladding region of the HNLF increases its MFD in the hot zone and reduces the transmission loss.

3. Experimental results

Figure 5 presents the SC spectra generated in the six investigated nonlinear fibers together with measurements of the respective spectrally resolved RIN. All measurements were obtained with identical pumping conditions with a coupled pump peak power of 33 kW and 110 fs pulse duration. The pulses were injected into HNLF-AD, HNLF-ND and HNLF-ANDi fibers either directly (left column) or in their respective hybrid version (right column). We obtained output SC average powers of 200 mW from the directly pumped HNLFs, which is reduced to about 160 mW from the hybrid fibers due to splice loss. The length of each fiber is adjusted individually in such a way that the full spectral bandwidth can develop, but short enough to avoid unnecessary spectral modulation and build-up of noise. The choice of fiber length is supported by numerical simulations further detailed in the discussion in Sec. 4.
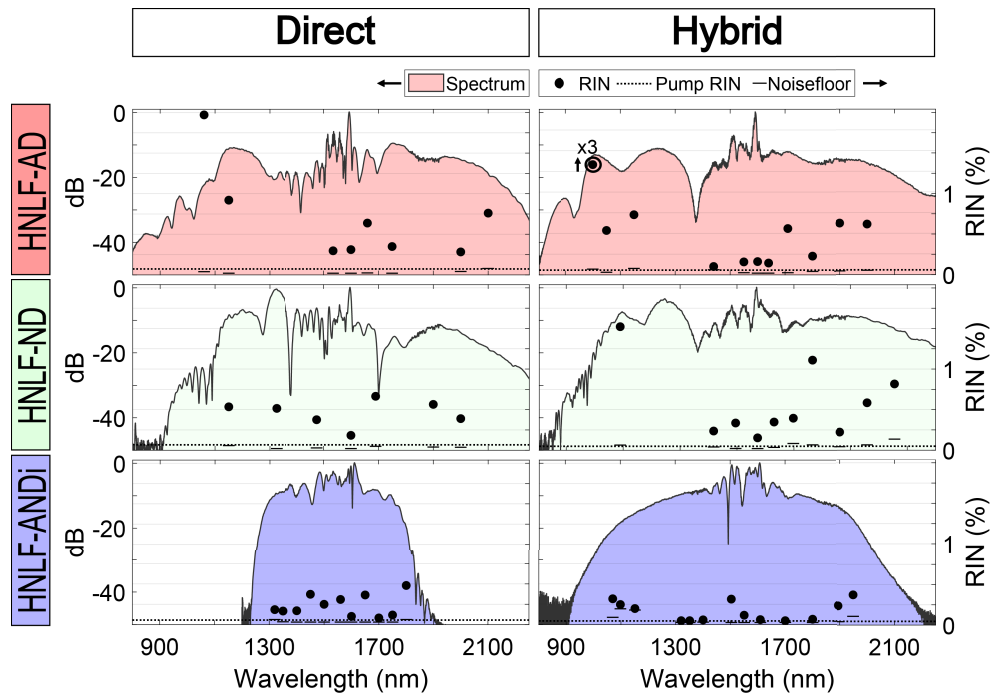

Fig. 5. Measured SC spectra generated in the six investigated nonlinear fibers and their spectrally resolved RIN under identical pumping conditions. Pump pulses were injected directly into HNLF (left column) or in their respective hybrid version (right column). Results for HNLF-AD, HNLF-ND, and HNLF-ANDi are shown in top, middle, and bottom row, respectively. RIN is measured for spectral slices of 20 nm width (dots) shown with respective noise floor (-) and compared to the pump laser RIN (0.05%, dashed line).

In general, we observe increased RIN levels near sharp spectral features, such as strong modulations or dips. This is due to the fact that the position of these features depends on the total nonlinear phase shift linked to the pump peak power, such that small pump fluctuations are translated to a relatively large change in SC signal. Hence, sharp spectral features generally act as amplifier of input intensity noise, and constitute an important link between flatness and noise level of SC sources.

For HNLF-AD, Fig. 5(a) and (b), the hybrid fiber generates SC spectra with significantly less fine structure, overall improved spectral flatness, and increased -30 dB spectral bandwidth (176 THz vs. 150 THz). The spectra feature a broad and smooth soliton structure around 2

µm and a massive dispersive wave extending from 1.35 µm down to below 1 µm wavelength, whose position can be tuned by controlling input pulse chirp [19]. In contrast, in the SC spectra emitted by the directly pumped fiber these features are narrower and exhibit stronger spectral modulation. However, the spectrally resolved RIN measurements result in similar values for both fibers, ranging mostly between 0.25 - 1%. Near the pump wavelength we observe a noise reduction in the hybrid fiber SC to 0.1 - 0.2 %, while the short wavelength dispersive wave peak generally exhibits higher noise, reaching 2% for the directly pumped fiber and increasing to 4% in the hybrid fiber, which corresponds to nearly 80 times amplification of the pump laser noise.

Although HNLF-ND exhibits normal dispersion at the pump wavelength, nonlinear self-phase modulation dynamics quickly transfer significant energy to the anomalous dispersion region, where dynamics are very similar to HNLF-AD discussed above, both for the directly pumped and the hybrid fiber. This is evident from the measured spectra shown in Fig. 5(c) and (d), which generally resemble the spectra generated in HNLF-AD, but are slightly narrower on the short wavelength edge and, in the case of the directly pumped fiber, even more strongly modulated. The effect of the hybrid approach is also very similar to the previous discussion: we observe a general reduction in spectral fine structure, improved spectral flatness, and an increase in -30 dB spectral bandwidth from 142 to 173 THz. It is interesting to note that pumping on the normal dispersion side of the ZDW does not have a notable benefit for the stability of the SC, except for the absence of the singular very high noise peaks. In fact, for the conditions investigated in this work there is hardly any significant advantage of HNLF-ND over HNLF-AD, with the latter producing broader SC bandwidth, similar spectral shapes, and similar noise levels.

HNLF-ANDi, Fig. 5(e) and (f), clearly benefits the most of all tested fibers from the hybrid approach, which approximately doubles the generated spectral bandwidth in comparison to the directly pumped fiber (145 THz vs. 75 THz, measured at -30 dB). We note that a further optimization of the soliton compression stage increases this bandwidth to over 180 THz [20], which easily competes with the bandwidths generated in the other investigated fibers. The hybrid HNLF-ANDi generates the flattest SC spectrum in this study, particularly below 1400 nm and above 1700 nm. In this case we also observe a significant noise reduction in the hybrid version of the fiber. Although the non-hybrid HNLF-ANDi generates the SC with the lowest RIN of all directly pumped HNLF, ranging between 0.1 - 0.5%, this still corresponds to an amplification of the pump laser noise by up to an order of magnitude. In contrast, this noise amplification is suppressed in the hybrid fiber, resulting in a SC with exceptionally low variation with wavelength. RIN is essentially equal to the pump laser noise near 0.05% for most of the measurement points, averaging <0.1% between 1150 - 1900 nm. RIN increases only at the spectral edges to 0.3-0.4% due to a drop in signal level.

4. Discussion

The benefit of the hybrid fiber approach for HNLF-AD and HNLF-ND is apparently limited to an improved spectral flatness and increased bandwidth, while the noise properties do not change significantly. In contrast, for the hybrid HNLF-ANDi we observe not only a doubling of spectral bandwidth in comparison to direct pumping, but also a significant reduction of RIN down to the limit given by the pump laser, which is on average a factor 5 – 10 lower than in the other tested cases.

In this section we show that these observations can be explained by the temporal characteristics of the pump pulses at the point of maximum compression reached during propagation in the fiber, which have a decisive influence over the spectral bandwidth, flatness, and noise characteristics of the resulting SC. We do this using numerical simulations for HNLF-AD and HNLF-ANDi. Since the dynamics for HNLF-ND are qualitatively very similar to HNLF-AD, we do not discuss a separate set of simulations for this case.

4.1. Spectral bandwidth and flatness

Figure 6 compares the simulated nonlinear spectral evolution in HNLF-AD for both direct-pumping and hybrid approaches. Although the injected pump pulses undergo soliton compression in both fibers, the nonlinear dynamics are quite different. Temporal compression and SC generation occur simultaneously in the directly pumped fiber, while in the hybrid version these processes occur largely separated in the two discrete fibers optimized for each task.
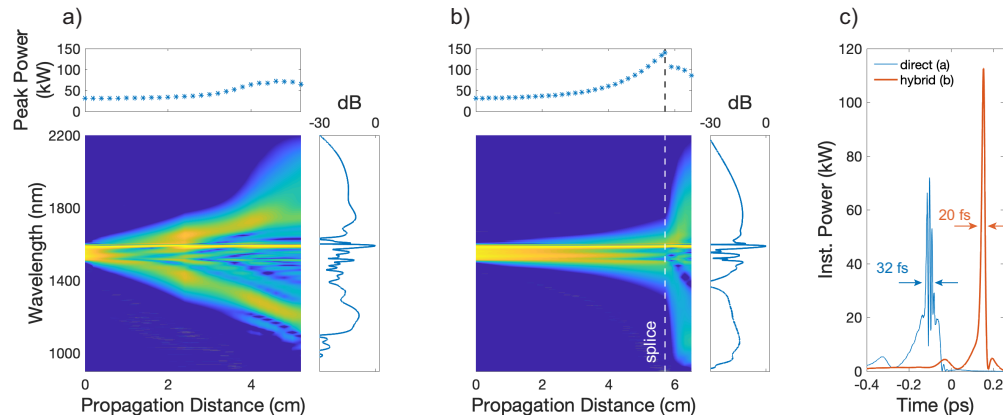

Fig. 6. Numerical simulation of the nonlinear spectral evolution in HNLF-AD fiber using (a) direct pumping and (b) the hybrid version of the fiber. The top projections show the evolution of pulse peak power, while the right projections show the the spectrum at the exit of the fiber. (c) Temporal pulse shape at the point of maximum compression for both fibers, which occurs at a propagation distance of 4.2 cm in case of direct pumping in (a) and 5.7 cm in the hybrid version in (b), where splice losses are taken into account. The input pulse properties are modeled after the experimental conditions and are identical in both cases.

Soliton compression takes place in the hybrid fiber with a nearly ideal soliton number of $N \simeq 4$, which leads to a much better quality of the compressed pulse as compared to the case of directly injecting the pump pulses into HNLF-AD, where they form a soliton of order $N \simeq 17$. This is evident from the comparison of the pulse shapes at the point of maximum compression in both fibers shown in Fig. 6(c). The high quality compression in the hybrid fiber produces a cleaner pulse shape concentrating more energy in the central pulse peak and, therefore, producing higher peak power even after splice losses are taken into account (120 kW vs. 70 kW). This directly explains the increased SC bandwidth generated with the hybrid fiber approach. The cleaner pulse shape is also the reason for the reduced spectral modulation observed in the hybrid fiber SC, because any form of temporal imperfections directly translate to strong spectral interference structures in the generated SC [30].

The same arguments can be made for HNLF-ANDi, which clearly benefits the most of all tested fibers from the hybrid concept. The corresponding simulations are shown in Fig. 7. The directly pumped fiber does not induce any mechanisms of pulse compression and, hence, the maximum peak power is available at the input and then drops continuously during propagation in the fiber. This generates the narrowest SC spectral bandwidth in our study. In contrast, the initial soliton compression in the hybrid fiber increases the peak power at the point of maximum compression from 33 kW to about 120 kW by a factor of 3.6. The spectral bandwidth $\Delta\omega$ of ANDi SC can be analytically related to the peak power P_0 of the pump pulse via $\Delta\omega \propto \sqrt{P_0}$ [31], such that we expect an increase of $\Delta\omega$ by a factor of 1.9 in the hybrid fiber, which is in excellent agreement with the experiment. The quality of the pulses at the point of maximum compression shown in Fig. 7(c) is similar, resulting also in very similar flatness of the generated

SC spectra. While ANDi fibers generally produce much smoother and flatter SC spectra than their conventional counterparts, in this case there are spectral modulations present near the center in both direct pumping and hybrid approaches. These features are well reproduced in the simulations and can be identified as spectral interference structures caused by low-level temporal side peaks and pedestals of the pump pulse [30].
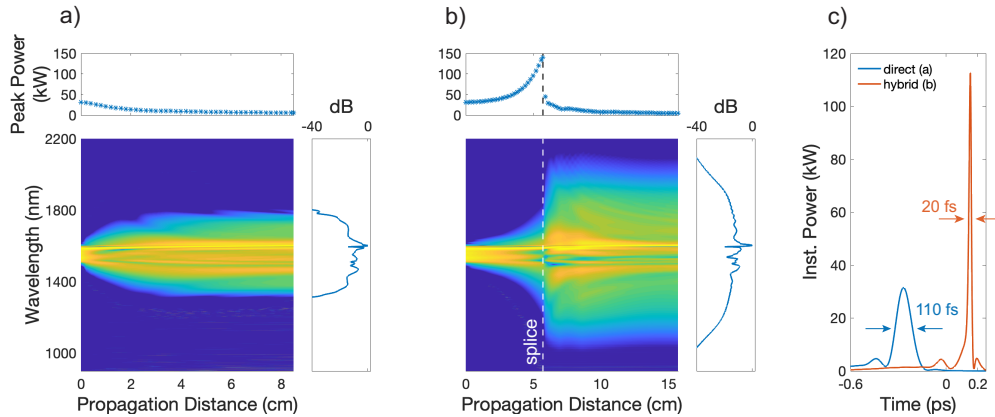

Fig. 7. Numerical simulation of the nonlinear spectral evolution in HNLF-ANDi fiber using (a) direct pumping and (b) the hybrid version of the fiber. (c) Minimum pulse duration encountered during propagation in both fibers, which corresponds to the input pulse in case of direct pumping in (a) and to the compressed soliton at 5.7 cm in the hybrid version in (b), where splice losses are taken into account. The input pulse properties are modelled after the experimental conditions and are identical in both cases.

4.2. Noise properties

The noise properties of the generated SC depend both on fiber and input pulse properties. However, when a given fiber is considered, a shorter pulse generally produces a more stable and coherent SC spectrum in any fiber design [16,25].

For HNLF-AD the injected pump pulses reach a very similar duration at the point of maximum compression in directly pumped and hybrid fibers, as shown in Fig. 6(c), despite the differences in pulse quality. Hence, the noise properties of the subsequently generated SC remain similar as well.

The situation is different for HNLF-ANDi. In this case we observe a significant noise reduction in the hybrid version of the fiber, which we can trace back to the strong temporal compression of the injected pulse. Previous research has related the elevated RIN level of up to 0.5% in the directly pumped fiber to the occurrence of incoherent polarization modulation instability (PMI) [20], facilitated by the relatively low birefringence of HNLF-ANDi (see Table 1). Whether or not PMI-amplified noise becomes significant mainly depends on the strength of the competing OWB-driven coherent nonlinear dynamics [32]. With direct pumping, the coherent dynamics are relatively slow and require about 3 cm of propagation through the fiber before spectral broadening is concluded, as shown in Fig. 7(a). This is sufficiently long for PMI to simultaneously amplify noise from the shot noise level. In the hybrid fiber however, the pump pulses enter HNLF-ANDi with just 20 fs duration, which leads to extremely fast coherent dynamics occurring on the scale of just 1 mm after the splice, as shown in Fig. 7(b). This suppresses PMI and prevents the accumulative build-up of noise. As a result, no significant noise amplification occurs during spectral broadening and the SC RIN drops to the limit given by the pump laser noise. We note that

these dynamics also lead to excellent phase-coherence of the generated SC, as was demonstrated in previous research [20].

It is interesting to directly compare the noise levels achieved in the three different hybrid fibers. In all of these cases, the pulse at the point of maximum compression is identical, namely the compressed $\sim$ 20 fs soliton delivered at the end of the SMF section. Under these conditions only the fiber design determines the noise properties of the generated SC. As is evident from our measurements, the SC generated in the hybrid ANDi HNLF exhibits on average significantly lower noise than can be obtained in the other hybrid HNLF with conventional dispersion design pumped near their ZDW. This experimentally confirms the theoretical considerations presented in Ref. [1] suggesting that the gain for noise-amplifying nonlinear effects in ANDi fibers is suppressed by up to one order magnitude with respect to fibers in which a significant part of the SC spectrum overlaps with the anomalous dispersion regime.

4.3. HNLF lengths

While the length of the SMF section for the hybrid fibers is carefully optimized via cutback measurements, as discussed in Section 2.3, the simulations in Figs. 6 and 7 are useful for determining the correct lengths of the HNLF sections used for experiments. For HNLF-AD choosing the correct length is critical. The fiber should be cut just after the maximum spectral broadening is obtained, i.e. to a length of 5 cm in the directly pumped case and about 1 cm for the hybrid fiber. In both cases the use of a longer HNLF section would induce stronger spectral modulations and higher noise without increasing spectral bandwidth. The same is valid for HNLF-ND, where slower nonlinear dynamics require slightly longer fiber lengths (8.5 cm for the directly pumped fiber and 2 cm for the hybrid fiber).

However, the opposite is true for HNLF-ANDi: using a longer HNLF section can be beneficial for improving flatness and noise properties. This is due to the fact that nonlinear OWB dynamics continue to reorder spectral components to unique temporal positions within the SC pulse even after spectral broadening ceases [33]. This flattens the spectrum by reducing spectral interference and reduces noise associated with sharp spectral features. However, care must be taken not to use excessive fiber lengths, as this can lead to the onset of incoherent dynamics, coherence collapse, and increasing noise levels [25]. We choose 8.5 cm for the directly pumped fiber and 20 cm for the hybrid fiber.

5. Conclusion

We present a comprehensive study of the benefits of cascaded nonlinear dynamics in hybrid fibers for the most common HNLF dispersion designs used for SC generation. Although the advantage of the hybrid approach is evident for all tested HNLF, the nature and degree of this benefit depend on the dispersion design of the particular fiber. Complementary numerical simulations highlight the fact that bandwidth, flatness, and noise of the generated SC depend critically on the peak power, quality, and duration of the pump pulses, respectively, reached at the point of maximum compression during propagation in the fiber.

Especially the hybrid ANDi HNLF stands out in our study as it combines the most beneficial aspects of nonlinear dynamics in both dispersion regimes. As a result of cascading nonlinear soliton compression with optical wavebreaking dynamics, it unites broad spectral bandwidth, superior flatness, and extremely low noise in a single low-cost solution. Using only commercial step-index polarization maintaining fibers, the hybrid approach avoids the complications associated with sourcing and integration of more complex photonic crystal fiber designs. In contrast, for HNLF with conventional dispersion design pumped near their ZDW, either in normal or anomalous dispersion regime, the benefit of the hybrid approach is limited to an improved spectral flatness and increased bandwidth, while they exhibit on average about an order of magnitude higher noise with much stronger wavelength dependence than can be obtained with the hybrid ANDi HNLF.

The hybrid approach can be readily adapted to a wide range of laser platforms and facilitate the scaling of low-noise SC sources to high repetition rates where the peak power per pulse is limited. While our work shows that few-cycle pulses are necessary to obtain the lowest noise levels, the hybrid fiber approach avoids the complexities associated with the careful optimization of laser and amplifier designs required for direct emission of such very short pulses [34,35]. Instead, both high quality nonlinear pulse compression to the few-cycle regime and octave-spanning SC generation with unprecedented low noise levels are obtainable from a single, external device. Virtually any available ultrafast laser source can benefit from optimized soliton compression with $N \simeq 5$ by selecting a pre-compression fiber with suitable nonlinearity and dispersion from the wide range of SMF and HNLF available from several manufacturers. Similarly, choosing an ANDi fiber with dispersion closer to zero could further enhance OWB-dominated spectral broadening. Hence, hybrid fibers are simple and easily reproducible solution for obtaining broadband spectra in wide range of high-precision laser applications where intensity and phase stability critically matter, including frequency comb spectroscopy, synchronization of ultrafast light sources, photonic radars, coherent optical communications, and photonic signal processing.

Disclosures. The authors declare no conflict of interest.

Data availability. The data underlying the results in this paper are available in Ref. [36].

References

1. A. Rampur, D.-M. Spangenberg, B. G. A. Sierro, P. M. Hänzi, M. Klimczak, and A. Heidt, "Perspective on the next generation of ultra-low noise fiber supercontinuum sources and their emerging applications in spectroscopy, imaging, and ultrafast photonics," Appl. Phys. Lett. **118**(24), 240504 (2021).
2. T. Sylvestre, E. Genier, A. N. Ghosh, P. Bowen, G. Genty, J. Troles, A. Mussot, A. C. Peacock, M. Klimczak, A. M. Heidt, J. C. Travers, O. Bang, and J. M. Dudley, "Recent advances in supercontinuum generation in specialty optical fibers [invited]," J. Opt. Soc. Am. B **38**(12), F90 (2021).
3. P. Abdolghader, A. F. Pegoraro, N. Y. Joly, A. Ridsdale, R. Lausten, F. Légaré, and A. Stolow, "All normal dispersion nonlinear fibre supercontinuum source characterization and application in hyperspectral stimulated Raman scattering microscopy," Opt. Express **28**(24), 35997–36008 (2020).
4. K. J. Kaltenecker, S. R. D. S. , M. Rasmussen, H. B. Lassen, E. J. R. Kelleher, E. Krauss, B. Hecht, N. A. Mortensen, L. Gruener-Nielsen, C. Markos, O. Bang, N. Stenger, and P. U. Jepsen, "Near-infrared nanospectroscopy using a low-noise supercontinuum source," APL Photonics **6**(6), 066106 (2021).
5. S. Rao D.S., M. Jensen, L. Grüner-Nielsen, J. T. Olsen, P. Heiduschka, B. Kemper, J. Schnekenburger, M. Glud, M. Mogensen, N. M. Israelsen, and O. Bang, "Shot-noise limited, supercontinuum-based optical coherence tomography," Light: Sci. Appl. **10**(1), 133 (2020).
6. H. Tu, Y. Liu, D. Turchinovich, M. Marjanovic, J. K. Lyngsø, J. Laegsgaard, E. J. Chaney, Y. Zhao, S. You, W. L. Wilson, B. Xu, M. Dantus, and S. A. Boppart, "Stain-free histopathology by programmable supercontinuum pulses," Nat. Photonics **10**(8), 534–540 (2016).
7. K. P. Herdzik, K. N. Bourdakos, P. B. Johnson, A. P. Lister, A. P. Pitera, C.-y. Guo, P. Horak, D. J. Richardson, J. H. Price, and S. Mahajan, "Multimodal spectral focusing CARS and SFG microscopy with a tailored coherent continuum from a microstructured fiber," Appl. Phys. B **126**(5), 84 (2020).
8. A. M. Heidt, J. M. Hodasi, A. Rampur, D.-M. Spangenberg, M. Ryser, M. Klimczak, and T. Feurer, "Low noise all-fiber amplification of a coherent supercontinuum at 2 μm and its limits imposed by polarization noise," Sci. Rep. **10**(1), 16734 (2020).
9. E. Temprana, E. Myslivets, B.-P. Kuo, L. Liu, V. Ataie, N. Alic, and S. Radic, "Overcoming Kerr-induced capacity limit in optical fiber transmission," Science **348**(6242), 1445–1448 (2015).
10. R. Sohanpal, H. Ren, L. Shen, C. Deakin, A. M. Heidt, T. W. Hawkins, J. Ballato, U. J. Gibson, A. C. Peacock, and Z. Liu, "All-fibre heterogeneously-integrated frequency comb generation using silicon core fibre," Nat. Commun. **13**(1), 3992 (2022).
11. M. Lippl, M. H. Frosz, and N. Y. Joly, "Low-noise supercontinuum generation in chiral all-normal dispersion photonic crystal fibers," arXiv, arXiv:2208.08357 (2022).
12. E. Genier, S. Grelet, R. D. Engelsholm, P. Bowen, P. M. Moselund, O. Bang, J. M. Dudley, and T. Sylvestre, "An ultra-flat, low-noise and linearly polarized fiber supercontinuum source covering 670 nm-1390 nm," Opt. Lett. **46**(8), 1820–1823 (2021).

13. S. Rao D.S., R. D. Engelsholm, I. B. Gonzalo, B. Zhou, P. Bowen, P. M. Moselund, O. Bang, and M. Bache, "Ultra-low-noise supercontinuum generation with a flat near-zero normal dispersion fiber," Opt. Lett. **44**(9), 2216–2219 (2019).

14. K. Tarnowski, T. Martynkien, P. Mergo, K. Poturaj, A. Anuszkiewicz, P. Béjot, F. Billard, O. Faucher, B. Kibler, and W. Urbanczyk, "Polarized all-normal dispersion supercontinuum reaching 2.5 μm generated in a birefringent microstructured silica fiber," Opt. Express **25**(22), 27452–27463 (2017).

15. M. Klimczak, B. Siwicki, A. Heidt, and R. Buczyński, "Coherent supercontinuum generation in soft glass photonic crystal fibers," Photonics Res. **5**(6), 710–727 (2017).

16. J. M. Dudley, G. Genty, and S. Coen, "Supercontinuum generation in photonic crystal fiber," Rev. Mod. Phys. **78**(4), 1135–1184 (2006).

17. G. Genty, S. Coen, and J. M. Dudley, "Fiber supercontinuum sources (invited)," J. Opt. Soc. Am. B **24**(8), 1771–1785 (2007).

18. T. Hori, J. Takayanagi, N. Nishizawa, and T. Goto, "Flatly broadened, wideband and low noise supercontinuum generation in highly nonlinear hybrid fiber," Opt. Express **12**(2), 317–324 (2004).

19. D. Brida, G. Krauss, A. Sell, and A. Leitenstorfer, "Ultrabroadband Er:fiber lasers," Laser Photonics Rev. **8**(3), 409–428 (2014).

20. B. Sierro, P. Hänzi, D. Spangenberg, A. Rampur, and A. M. Heidt, "Reducing the noise of fiber supercontinuum sources to its limits by exploiting cascaded soliton and wave breaking nonlinear dynamics," Optica **9**(4), 352–359 (2022).

21. D.-M. Spangenberg, B. Sierro, A. Rampur, P. Hänzi, A. Hartung, P. Mergo, K. Tarnowski, T. Martynkien, M. Klimczak, and A. M. Heidt, "Noise fingerprints of fiber supercontinuum sources," in *2021 Conference on Lasers and Electro-Optics Europe and European Quantum Electronics Conference*, (Optica Publishing Group, 2021), p. cd_5_3.

22. R. P. Scott, C. Langrock, and B. H. Kolner, "High-dynamic-range laser amplitude and phase noise measurement techniques," IEEE J. Sel. Top. Quantum Electron. **7**(4), 641–655 (2001).

23. J. Kim and Y. Song, "Ultralow-noise mode-locked fiber lasers and frequency combs: principles, status, and applications," Adv. Opt. Photonics **8**(3), 465 (2016).

24. P. Ciąćka, A. Rampur, A. Heidt, T. Feurer, and M. Klimczak, "Dispersion measurement of ultra-high numerical aperture fibers covering thulium, holmium, and erbium emission wavelengths," J. Opt. Soc. Am. B **35**(6), 1301–1307 (2018).

25. A. M. Heidt, J. S. Feehan, J. H. V. Price, and T. Feurer, "Limits of coherent supercontinuum generation in normal dispersion fibers," J. Opt. Soc. Am. B **34**(4), 764–775 (2017).

26. C.-M. Chen and P. L. Kelley, "Nonlinear pulse compression in optical fibers: scaling laws and numerical analysis," J. Opt. Soc. Am. B **19**(9), 1961–1967 (2002).

27. A. M. Heidt, D.-M. Spangenberg, M. Brügmann, E. G. Rohwer, and T. Feurer, "Improved retrieval of complex supercontinuum pulses from XFROG traces using a ptychographic algorithm," Opt. Lett. **41**(21), 4903–4906 (2016).

28. T. Godin, B. Wetzel, T. Sylvestre, L. Larger, A. Kudlinski, A. Mussot, A. B. Salem, M. Zghal, G. Genty, F. Dias, and J. M. Dudley, "Real time noise and wavelength correlations in octave-spanning supercontinuum generation," Opt. Express **21**(15), 18452–18460 (2013).

29. B. Sierro and A. M. Heidt, "Noise amplification in all-normal dispersion fiber supercontinuum generation and its impact on ultrafast photonics applications," OSA Continuum **3**(9), 2347–2361 (2020).

30. A. Rampur, D.-M. Spangenberg, G. Stepniewski, D. Dobrakowski, K. Tarnowski, K. Stefanska, A. Pazdzior, P. Mergo, T. Martynkien, T. Feurer, M. Klimczak, and A. M. Heidt, "Temporal fine structure of all-normal dispersion fiber supercontinuum pulses caused by non-ideal pump pulse shapes," Opt. Express **28**(11), 16579–16593 (2020).

31. A. M. Heidt, D. Spangenberg, A. Rampur, A. Hartung, and H. Bartelt, The Supercontinuum Laser Source (Springer, 2022), chap. All-Normal Dispersion Fiber Supercontinuum: Principles, Design, and Applications of a Unique White Light Source, pp. 299–341.

32. I. B. Gonzalo, R. D. Engelsholm, M. P. Sørensen, and O. Bang, "Polarization noise places severe constraints on coherence of all-normal dispersion femtosecond supercontinuum generation," Sci. Rep. **8**(1), 6579 (2018).

33. A. M. Heidt, A. Hartung, G. W. Bosman, P. Krok, E. G. Rohwer, H. Schwoerer, and H. Bartelt, "Coherent octave spanning near-infrared and visible supercontinuum generation in all-normal dispersion photonic crystal fibers," Opt. Express **19**(4), 3775–3787 (2011).

34. J. Sotor and G. Sobon, "24 fs and 3 nJ pulse generation from a simple, all polarization maintaining Er-doped fiber laser," Laser Phys. Lett. **13**(12), 125102 (2016).

35. H. Luo, L. Zhan, L. Zhang, Z. Wang, C. Gao, and X. Fang, "Generation of 22.7-fs 2.8-nJ pulses from an Erbium-doped all-fiber laser via single-stage soliton compression," J. Lightwave Technol. **35**(17), 3780–3784 (2017).

36. P. Hänzi, B. Sierro, Z. Liu, V. Romano, A. Rampur, and A. M. Heidt, "Dataset: Benefits of cascaded nonlinear dynamics in hybrid fibers for low-noise supercontinuum generation," *Bern Open Research and Information System (BORIS)* (2023), https://doi.org/10.48620/218.